IJC
International Journal of Cancer

MicroRNA-31 expression in relation to *BRAF* mutation, CpG island methylation and colorectal continuum in serrated lesions

Miki Ito[1*], Kei Mitsuhashi[1*], Hisayoshi Igarashi[1*], Katsuhiko Nosho[1], Takafumi Naito[1], Shinji Yoshii[2,3], Hiroaki Takahashi[2], Masahiro Fujita[4], Yasutaka Sukawa[1], Eiichiro Yamamoto[1,5], Taiga Takahashi[1], Yasushi Adachi[1], Masanori Nojima[6], Yasushi Sasaki[7], Takashi Tokino[7], Yoshifumi Baba[8], Reo Maruyama[5], Hiromu Suzuki[5], Kohzoh Imai[6], Hiroyuki Yamamoto[9†] and Yasuhisa Shinomura[1†]

[1] Department of Gastroenterology, Rheumatology and Clinical Immunology, Sapporo Medical University School of Medicine, Sapporo, Japan
[2] Department of Gastroenterology, Keiyukai Sapporo Hospital, Sapporo, Japan
[3] Department of Gastroenterology, NTT East Sapporo Hospital, Sapporo, Japan
[4] Department of Pathology, Keiyukai Sapporo Hospital, Sapporo, Japan
[5] Department of Molecular Biology, Sapporo Medical University School of Medicine, Sapporo, Japan
[6] The Institute of Medical Science, The University of Tokyo, Tokyo, Japan
[7] Department of Medical Genome Sciences, Research Institute for Frontier Medicine, Sapporo Medical University School of Medicine, Sapporo, Japan
[8] Department of Gastroenterological Surgery, Graduate School of Medical Science, Kumamoto University, Kumamoto, Japan
[9] Division of Gastroenterology and Hepatology, Department of Internal Medicine, St. Marianna University School of Medicine, Kawasaki, Japan

The CpG island methylator phenotype (CIMP) is a distinct form of epigenomic instability. Many CIMP-high colorectal cancers (CRCs) with *BRAF* mutation are considered to arise from serrated pathway. We recently reported that microRNA-31 (miR-31) is associated with *BRAF* mutation in colorectal tumors. Emerging new approaches have revealed gradual changes in *BRAF* mutation and CIMP-high throughout the colorectum in CRCs. Here, we attempted to identify a possible association between miR-31 and epigenetic features in serrated pathway, and hypothesized that miR-31 supports the "colorectal continuum" concept. We evaluated miR-31 expression, *BRAF* mutation and epigenetic features including CIMP status in 381 serrated lesions and 222 non-serrated adenomas and examined associations between them and tumor location (rectum; sigmoid, descending, transverse and ascending colon and cecum). A significant association was observed between high miR-31 expression and CIMP-high status in serrated lesions with *BRAF* mutation ($p = 0.0001$). In contrast, miR-31 was slightly but insignificantly associated with CIMP status in the cases with wild-type *BRAF*. miR-31 expression in sessile serrated adenomas (SSAs) with cytological dysplasia was higher than that in SSAs, whereas, no significant difference was observed between traditional serrated adenomas (TSAs) and TSAs with high-grade dysplasia. The frequency of miR-31, *BRAF* mutation CIMP-high and *MLH1* methylation increased gradually from the rectum to cecum in serrated lesions. In conclusion, miR-31 expression was associated with CIMP-high status in serrated lesions with *BRAF* mutation. Our data also suggested that miR-31 plays an important role in SSA evolution and may be a molecule supporting the colorectal continuum.

Key words: *BRAF*, CIMP, colon, miR-31, serrated polyp

Abbreviations: CIMP: CpG island methylator phenotype; CRC: colorectal cancer; FFPE: formalin-fixed paraffin-embedded; HGD: high-grade dysplasia; HP: hyperplastic polyp; miRNA: microRNA; miR-31: microRNA-31; MSI: microsatellite instability; MSS: microsatellite stable; qRT-PCR: quantitative reverse transcription-polymerase chain reaction; SSA: sessile serrated adenoma; TSA: traditional serrated adenoma

Additional Supporting Information may be found in the online version of this article.

*M.I., K.M. and H.I. contributed equally to this work

†HY and YS contributed equally to this work

Grant sponsor: Japan Society for the Promotion of Science (JSPS) Grant-in-Aid for Scientific Research; **Grant number:** 23790800; **Grant sponsors:** A-STEP (Adaptable and Seamless Technology Transfer Program through Target-driven R&D), Takeda Science Foundation, Daiwa Securities Health Foundation

DOI: 10.1002/ijc.28920

History: Received 25 Jan 2014; Accepted 9 Apr 2014; Online 20 Apr 2014

Correspondence to: Katsuhiko Nosho, Department of Gastroenterology, Rheumatology and Clinical Immunology, Sapporo Medical University School of Medicine, S-1, W-16, Chou-ku, Sapporo, 060-8543, Japan. Tel: +81-11-611-2111, Fax: +81-11-611-2282, E-mail: nosho@sapmed.ac.jp

What's new?

The serrated neoplasia pathway has attracted considerable attention as an alternative route for colorectal cancer development. This study shows that high microRNA-31 expression is associated with CpG island methylator phenotype (CIMP)-high status in serrated lesions with *BRAF* mutation. The data also indicate that miR-31 may play a role in sessile serrated adenoma evolution. Moreover, not only do *BRAF* mutation and CIMP-high status increase gradually from the rectum to the caecum but high miR-31 expression does, too, suggesting that miR-31 is a key molecule in the colorectal continuum concept. These novel data shed light on details of the colorectal serrated pathway.

The serrated neoplasia pathway has attracted considerable attention as an alternative pathway of colorectal cancer (CRC) development, and serrated lesions exhibit unique clinicopathological or molecular features.[1–17] The CpG island methylator phenotype (CIMP) is a distinct form of epigenomic instability,[18–22] which causes most sporadic microsatellite instability (MSI)-high CRCs through epigenetic inactivation of *MLH1*.[23] Independent of MSI, CIMP-high CRCs are associated with proximal tumor location, old age of onset, female gender and *BRAF* mutation.[20,21] In particular, there are many clinicopathological and molecular similarities between sessile serrated adenomas (SSAs) and CIMP-high CRC, for example proximal tumor location, *BRAF* mutation and *MLH1* methylation.[4,9,24–29] Therefore, SSAs are hypothesized to be precursor lesions that develop into CIMP-high CRCs with *BRAF* mutation in the proximal colon.[4,9,24,25,27,30]

MicroRNAs (miRNAs) constitute a class of small non-coding RNA molecules that function as post-transcriptional gene regulators and have been increasingly recognized as useful biomarkers for CRC.[31–37] Using miRNA array analysis, we recently discovered that microRNA-31 (miR-31) expression is significantly up-regulated in *BRAF*-mutated CRCs compared with that in wild-type CRCs.[38] Moreover, associations were identified between miR-31 expression, proximal tumor location and poor prognosis for CRCs. With regard to premalignant colorectal lesions, high miR-31 expression is frequently detected in cases with serrated lesions compared to that in cases with non-serrated adenomas, suggesting an association between miR-31 expression and the serrated pathway.[38] Nevertheless, no previous study has reported an association between miR-31 expression and CIMP status or its role in the progression of serrated lesions.

CRC is typically classified into rectal, distal colon and proximal colon cancers. Some investigators believe that proximal colon cancers and distal cancers differ in clinical, pathological and molecular features (the 'two-colon' concept) [39–41]; however, it remains uncertain whether the molecular features of CRC change abruptly at the splenic flexure. On the other hand, a recent study has reported that the frequency of molecular features such as *BRAF* mutation, CIMP status and MSI increases gradually from the rectum to the ascending colon in CRCs (the 'colorectal continuum' concept).[20,41] However, no previous study has examined whether a gradual change in miR-31 expression is observed throughout the colorectum.

In this study, we attempted to identify a possible association of miR-31 expression with epigenetic features including CIMP status and its role in the progression of serrated lesions, and hypothesized that miR-31 may support the colorectal continuum concept in the serrated pathway. We examined miR-31 expression level as well as detailed tumor location and molecular features using 381 serrated lesions and 222 non-serrated adenomas.

Materials and Methods

Histopathological evaluation of tissue specimens of colorectal serrated lesions

Histological findings related to all colorectal serrated lesion specimens were evaluated by two pathologists (M.F. and S.Y.) who were blinded to the clinical and molecular information. Serrated lesions [hyperplastic polyps (HPs), sessile serrated adenomas (SSAs) and traditional serrated adenomas (TSAs)] were classified on the basis of the current World Health Organisation (WHO) criteria.[42] HPs were further subdivided into microvesicular HP and goblet cell HP. To accurately analyze the association between the histological types and molecular features of each type of serrated lesion ($N = 404$), we consecutively collected formalin-fixed paraffin-embedded (FFPE) tissue specimens. All HPs were found to be microvesicular HPs. Non-serrated adenomas (tubular or tubulovillous adenomas) ($N = 233$) and CRCs ($N = 870$) were analyzed as controls. Only one colorectal lesion per participant was analyzed. We collected and analyzed 1507 tissue specimens of colorectal serrated lesions, non-serrated adenomas and CRCs from patients who underwent endoscopic resection or surgical treatment at Sapporo Medical University Hospital or Keiyukai Sapporo Hospital between 2001 and 2013. Informed consent was obtained from all patients before specimen collection. This study was approved by the institutional review boards of the participating institutions.

RNA extraction and quantitative reverse transcription-polymerase chain reaction of miR-31

Total RNA was extracted from FFPE tissues using the miRNeasy FFPE Kit (Qiagen, Valencia, CA).[38] miR-31-5p expression was analyzed by quantitative reverse transcription-polymerase chain reaction using the TaqMan MicroRNA Reverse Transcription Kit (Applied Biosystems, Foster City, CA) and TaqMan microRNA Assays (Applied Biosystems) as

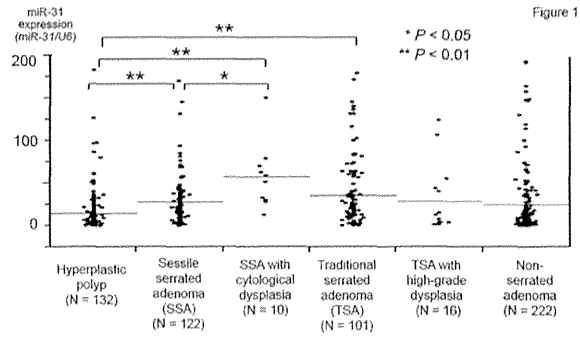

Figure 1. MicroRNA-31 (miR-31) expression (miR-31/U6) levels by histological type. miR-31 expression levels in sessile serrated adenomas (SSAs), SSAs with cytological dysplasia and traditional serrated adenomas (TSAs) was significantly higher than that in hyperplastic polyps (HPs). Moreover, a significant difference in the expression level was observed between sessile serrated adenoma (SSA) and SSA with cytological dysplasia. HP: hyperplastic polyp; miR-31: microRNA-31; SSA: sessile serrated adenoma; TSA: traditional serrated adenoma.

previously described.[38] The conditions for real-time PCR were as follows: 95°C for 10 min, followed by 40 cycles of 95°C for 15 sec and 60°C for 60 sec. PCR was run in triplicate on a 7500 fast real-time PCR System (Applied Biosystems). SDS v1.4 software (Applied Biosystems) was used for comparative analysis of the cycle threshold (ΔC_T). U6 snRNA (RNU6B; Applied Biosystems) served as an endogenous control. miR-31 expression was calculated using the equation: $2^{-\Delta CT}$, where $\Delta C_T = (C_T$ miR-31 $- C_T$ U6). To determine relative miR-31 expression in each serrated lesion or non-serrated adenoma, the $2^{-\Delta CT}$ value of tumor tissue was divided by that of normal tissue, as described previously.[38]

DNA extraction and pyrosequencing of *KRAS* and *BRAF* mutations and MSI analysis

Genomic DNA was extracted from FFPE tissues using the QIAamp DNA FFPE Tissue Kit (Qiagen).[38] Using the extracted genomic DNA, PCR and targeted pyrosequencing were performed for *KRAS* (codons 12 and 13) and *BRAF* (*V600E*).[43] MSI analysis was performed as previously described.[38]

Sodium bisulfite treatment and real-time PCR (MethyLight) to measure promoter methylation of *CACNA1G, CDKN2A (p16), IGF2, MGMT, MLH1* and *RUNX3*

Bisulfite modification of genomic DNA was performed using the BisulFlash™ DNA Modification Kit (Epigentek, Brooklyn, NY).[38] We quantified DNA methylation in four CIMP-specific promoters [*CACNA1G, CDKN2A* (*p16*), *IGF2* and *RUNX3*] and *MGMT* and *MLH1* using real-time PCR (MethyLight).[21] CIMP-high status was defined as the presence of three/four or more methylated promoters and CIMP low/zero as zero/four to two/four methylated promoters.

Statistical analysis

JMP (version 10) software was used for all statistical analyses (SAS Institute, Cary, NC). *p* Values were two-sided. Univariate analysis was performed to determine the clinicopathological and molecular characteristics including miR-31 expression according to the histological type of the serrated lesions or non-serrated adenomas. *p* Values were calculated using analysis of variance for age and tumor size and by chi-square or Fisher's exact test for all other variables. The chi-square test for linear trends was used when comparing the frequencies of *BRAF* mutations, CIMP-high status, *MLH1* and *MGMT* methylations and miR-31 expression in premalignant colorectal lesions found in the rectum, the sigmoid, descending, transverse and ascending colon and the cecum.

Multivariate logistic regression analysis was used to examine the association with miR-31 expression status (as an outcome variable), adjusting for potential confounders. The model initially included gender (male *vs.* female), age (continuous), tumor size (continuous), tumor location (proximal colon *vs.* distal colon and rectum), histological type (SSA and TSA *vs.* HP), CIMP status (CIMP-high *vs.* CIMP-low/zero), MSI (MSI-high *vs.* MSS/MSI-low), *BRAF* and *KRAS* mutations (present *vs.* absent) and *MGMT* and *MLH1* methylation (present *vs.* absent). A backward elimination procedure with a threshold of $p = 0.10$ was used to select variables in the final model. The *p* Value for significance was adjusted by Bonferroni correction to $p = 0.0045$ ($= 0.05/11$).

Results

MicroRNA-31 expression in serrated lesions and non-serrated adenomas

We assessed 637 FFPE tissue specimens of serrated lesions and nonserrated adenomas and 870 specimens of CRCs using the miR-31 expression assay and successfully obtained 603 (95%) and 841 (97%) positive results, respectively. Next miR-31 expression level was quantified in hyperplastic polyps (HPs) ($N = 132$), sessile serrated adenomas (SSAs) ($N = 122$), SSAs with cytological dysplasia ($N = 10$), traditional serrated adenomas (TSAs) ($N = 101$), TSAs with high-grade dysplasia (HGD; $N = 16$) and non-serrated adenomas ($N = 222$) and found to be 14.2 ± 26.5; 3.6 (mean $\pm$ SD; median) in HPs, 27.8 ± 37.1; 15.7 in SSAs, 57.5 ± 38.8; 55.3 in SSAs with cytological dysplasia, 36.0 ± 41.1; 19.8 in TSAs, 28.8 ± 38.3 in TSAs with HGD; 10.0, 21.8 ± 54.3; 3.5 in non-serrated adenomas and 33.6 ± 3.7; 6.2 in CRCs. miR-31 expression level in SSAs, SSAs with cytological dysplasia and TSAs was significantly higher than that in HPs ($p \leq 0.0013$; Fig. 1). Moreover, a significant difference in the expression level was observed between SSA and SSA with cytological dysplasia ($p = 0.017$).

The distribution of miR-31 expression in the 381 specimens of serrated lesions and 222 specimens of non-serrated adenomas was as follows: mean, 24.9; median, 7.3; SD, 50.0; range, 0.06–462.0 and interquartile range, 1.6–30.2. Cases with miR-31 expression were divided into quartiles Q1 (<1.6), Q2 (1.6–7.3), Q3 (7.4–30.2) and Q4 (≥30.2) for further analysis.

Table 1. MicroRNA-31 and clinicopathological and molecular features in serrated lesions and non-serrated adenomas

Clinicopathological or molecular features	Total (*N*)	MicroRNA-31 expression (quartile) Q1 (<1.6)	Q2 (1.6–7.3)	Q3 (7.4–30.1)	Q4 (≥30.2)	
All cases	**603**	**152**	**153**	**148**	**150**	*p*
Gender						
Male	362 (60%)	101 (66%)	85 (56%)	80 (54%)	96 (64%)	0.069
Female	241 (40%)	51 (34%)	68 (44%)	68 (46%)	54 (36%)	
Age (mean ± SD)	62.0 ± 12.1	63.1 ± 11.3	60.4 ± 12.7	62.4 ± 12.8	62.3 ± 11.5	0.26
Tumor size (mm) (mean ± SD)	14.1 ± 11.1	16.4 ± 13.3	13.3 ± 10.8	14.0 ± 10.5	12.6 ± 9.5	0.020
Tumor location						
Rectum	78 (13%)	38 (25%)	23 (15%)	6 (4.1%)	11 (7.3%)	< 0.0001
Sigmoid colon	149 (25%)	45 (30%)	47 (31%)	29 (20%)	28 (19%)	
Descending colon (including splenic flexure)	41 (6.8%)	12 (7.9%)	11 (7.2%)	10 (6.8%)	8 (5.3%)	
Transverse colon (including hepatic flexure)	114 (19%)	25 (16%)	37 (24%)	26 (18%)	26 (17%)	
Ascending colon	139 (23%)	25 (16%)	29 (19%)	45 (30%)	40 (27%)	
Cecum	82 (14%)	7 (4.6%)	6 (3.9%)	32 (22%)	37 (25%)	
Histopathology						
Hyperplastic polyps (HPs)	132 (22%)	39 (26%)	47 (31%)	27 (18%)	19 (13%)	< 0.0001
Sessile serrated adenomas (SSAs)	122 (20%)	10 (6.6%)	30 (20%)	44 (30%)	38 (25%)	
SSAs with cytological dysplasia	10 (1.7%)	0 (0%)	0 (0%)	2 (1.4%)	8 (5.3%)	
Traditional serrated adenomas (TSAs)	101 (17%)	11 (7.2%)	17 (11%)	33 (22%)	40 (27%)	
TSAs with high-grade dysplasia	16 (2.7%)	3 (2.0%)	5 (3.3%)	2 (1.4%)	6 (4.0%)	
Non-serrated adenomas (tubular or tubulovillous adenomas)	222 (37%)	89 (59%)	54 (35%)	40 (27%)	39 (26%)	
BRAF mutation						
Wild-type	354 (59%)	128 (84%)	95 (62%)	71 (48%)	60 (40%)	< 0.0001
Mutant	249 (41%)	24 (16%)	58 (38%)	77 (52%)	90 (60%)	
KRAS mutation						
Wild-type	463 (77%)	105 (69%)	115 (75%)	122 (82%)	121 (81%)	0.028
Mutant	140 (23%)	47 (31%)	38 (25%)	26 (18%)	29 (19%)	
CIMP status						
CIMP-low/zero	503 (83%)	138 (91%)	142 (93%)	118 (80%)	105 (70%)	< 0.0001
CIMP-high	100 (17%)	14 (9.2%)	11 (7.2%)	30 (20%)	45 (30%)	
MSI						
MSS/MSI-low	594 (99%)	151 (99%)	150 (98%)	146 (99%)	147 (98%)	0.71
MSI-high	9 (1.5%)	1 (0.7%)	3 (2.0%)	2 (1.4%)	3 (2.0%)	

Percentage (%) indicates the number of cases with a specific clinicopathological or molecular feature within a given quartile category (Q1, Q2, Q3 or Q4) of microRNA-31 expression. *p* Values were calculated by analysis of variance for age and tumor size and by chi-square or Fisher's exact test for all other variables. To account for multiple hypothesis testing in association between miR-31 expression and other nine covariates, the *P* value for significance was adjusted by Bonferroni correction to $p = 0.0056$ (= 0.05/9).
Abbreviations: CIMP: CpG island methylator phenotype; HP: hyperplastic polyp; MSI: microsatellite instability; MSS: microsatellite stable; SD: standard deviation; SSA: sessile serrated adenoma; TSA: traditional serrated adenoma.

Association of microRNA-31 expression and clinicopathological and molecular features in serrated lesions and non-serrated adenomas

Table 1 shows the clinicopathological and molecular features of serrated lesions and non-serrated adenomas according to the miR-31 expression level. miR-31 expression was significantly associated with tumor location, histopathology, *BRAF* mutation and CIMP-high status ($p < 0.0001$). No significant difference was observed between miR-31 expression and *KRAS* mutation ($p = 0.028$) or MSI ($p = 0.71$). When limiting cases to serrated lesions, miR-31 expression was associated with tumor location, histopathology, *BRAF* mutation and CIMP-high status ($p < 0.0001$; data not shown).

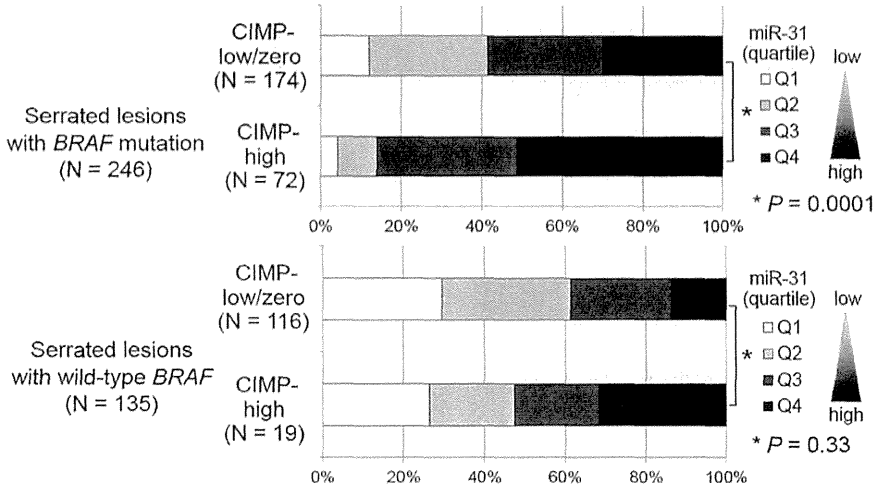

Figure 2. Association between miR-31 expression and CIMP status in relation to *BRAF* status in serrated lesions (HPs, SSAs, SSAs with cytological dysplasia, TSAs and TSAs with high-grade dysplasia). A significant association was observed between high miR-31 expression and CIMP-high status in serrated lesions with *BRAF* mutation. However, miR-31 expression was slightly but insignificantly associated with CIMP status in the cases with wild-type *BRAF*. Cases with miR-31 expression were divided into quartiles Q1 (<1.6), Q2 (1.6–7.3), Q3 (7.4–30.2) and Q4 (≥30.2). CIMP: CpG island methylator phenotype; HP: hyperplastic polyp; miR-31: microRNA-31; SSA: sessile serrated adenoma; TSA: traditional serrated adenoma.

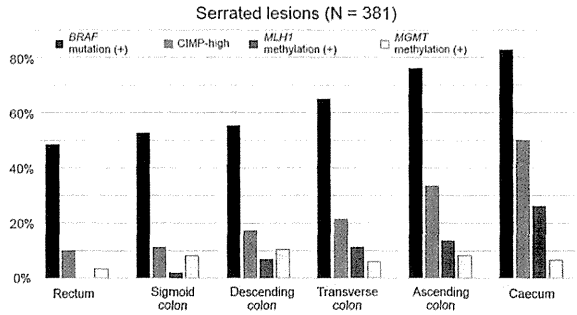

Figure 3. Frequency of *BRAF* mutation, CIMP-high and *MLH1* methylation in serrated lesions (HPs, SSAs, SSAs with cytological dysplasia, TSAs and TSAs with high-grade dysplasia). Frequency of *BRAF* mutation, CIMP-high and *MLH1* methylation increased gradually from the rectum to cecum in serrated lesions ($p \leq 0.0002$), but there was no significant difference between *MGMT* methylation and tumor location. CIMP: CpG island methylator phenotype; HP: hyperplastic polyp; SSA: sessile serrated adenoma; TSA: traditional serrated adenoma.

Association of miR-31 expression and *BRAF* mutation or CIMP status in serrated lesions

Because *BRAF* mutation has been tightly associated with CIMP-high status, we examined miR-31 expression in relation to *BRAF* and CIMP status. High miR-31 expression was associated with *BRAF* mutation and was independent of CIMP status in serrated lesions ($p \leq 0.017$; Supporting Information Fig. 1). In contrast, a significant association was observed between high miR-31 expression and CIMP-high status in serrated lesions with *BRAF* mutation ($p = 0.0001$; Fig. 2). However, miR-31 expression was slightly but insignificantly associated with CIMP status in the cases with wild-type *BRAF* ($p = 0.33$).

Multivariate analysis to identify association with miR-31 expression in serrated lesions

We also performed multivariate logistic regression analysis to confirm that the association between miR-31 expression and *BRAF* mutation or CIMP status was independent of any other clinical and molecular variables in serrated lesions. Our data showed that miR-31 expression was associated with *BRAF* mutation ($p = 0.0037$) and was independent of other variables (Supporting Information Table 1).

Molecular characteristics of serrated lesions according to tumor location

The frequency of *BRAF* mutation, CIMP-high status and *MLH1* methylation increased gradually from the rectum to cecum in serrated lesions ($p \leq 0.0002$), but there was no significant association between *MGMT* methylation and tumor location (Fig. 3). Similarly, the number of serrated lesions with high miR-31 expression increased gradually from the rectum to cecum ($p < 0.0001$; Fig. 4). Similar results were observed in non-serrated adenomas ($p < 0.0001$; Fig. 4) and CRCs ($p < 0.0001$; Supporting Information Fig. 2). After serrated lesions and non-serrated adenomas were stratified by *BRAF* mutation, the association between miR-31 expression and tumor location persisted ($p \leq 0.0011$; Supporting Information Fig. 3).

Association of miR-31 expression and molecular alteration in SSAs with or without cytological dysplasia

High miR-31 expression was conspicuous in SSAs with cytological dysplasia compared to that in SSAs ($p = 0.0079$; Table 2). CIMP-high was well pronounced in SSAs with cytological

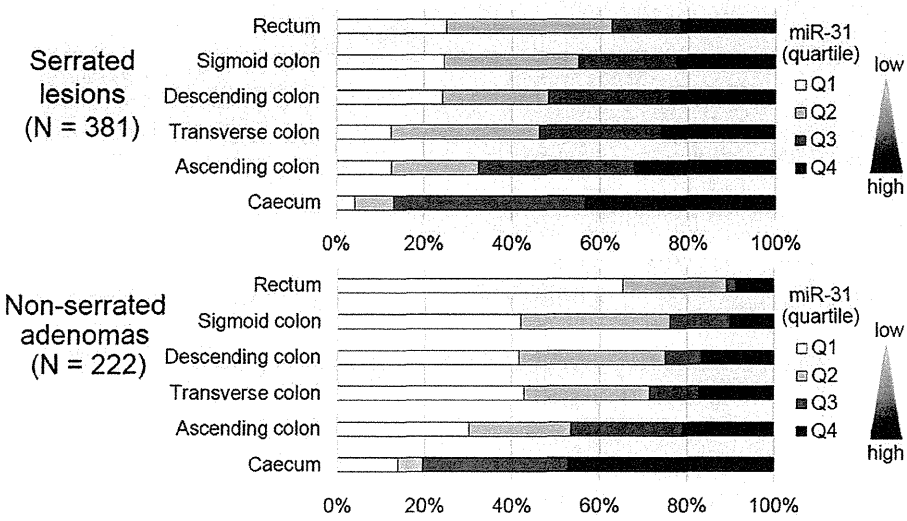

Figure 4. Frequency of miR-31 expression in serrated lesions (HPs, SSAs, SSAs with cytological dysplasia, TSAs and TSAs with high-grade dysplasia) or non-serrated adenomas (tubular or tubulovillous adenomas). The number of cases with high miR-31 expression increased gradually from the rectum to the cecum in not only in serrated lesions ($p < 0.0001$) but also in non-serrated adenomas ($p < 0.0001$). Cases with miR-31 expression were divided into quartiles Q1 (<1.6), Q2 (1.6–7.3), Q3 (7.4–30.2) and Q4 (≥30.2). HP: hyperplastic polyp; miR-31: microRNA-31; SSA: sessile serrated adenoma; TSA: traditional serrated adenoma.

dysplasia (100%, 10/10) compared to that in SSAs (38%, 46/122; $p < 0.0001$). *MLH-1* methylation was more frequently observed in SSAs with cytological dysplasia (80%, 8/10) than in SSAs (16%, 20/122; $p < 0.0001$). Likewise, *MGMT* methylation was more frequently observed in SSAs with cytological dysplasia (40%, 4/10) than in SSAs (7.4%, 9/122; $p = 0.0071$).

Association of miR-31 expression and molecular alteration in TSAs with or without HGD

With regard to TSAs, no significant difference in miR-31 expression was found between TSAs with HGD and TSAs ($p = 0.23$; Table 2). In contrast, CIMP-high status was more frequently detected in TSAs with HGD (75%, 12/16) than in TSAs (12%, 12/101; $p < 0.0001$). *MGMT* methylation was more frequently observed in TSAs with HGD (38%, 6/16) than in TSAs (3.0%, 3/101; $p < 0.0001$), but no significant difference in *MLH1* methylation was found between TSAs with HGD (0%, 0/16) and TSAs (4.0%, 4/101; $p = 0.27$).

Discussion

We performed this study to identify the possible association of miR-31 expression with epigenetic features including CIMP status as well as its role in the progression of serrated lesions. High miR-31 expression was associated with CIMP-high status in serrated lesions with *BRAF* mutation. Our data also showed that the association between miR-31 expression and *BRAF* mutation status was independent of CIMP status. Thus, this is the first report to identify an association between miR-31expression, *BRAF* mutations and CIMP status in serrated lesions. Moreover, high miR-31 expression was well pronounced in SSAs with cytological dysplasia than in SSAs, but no significant difference was observed between TSAs and TSAs with HGD. With regard to the colorectal continuum concept, the frequency of high miR-31 expression increased gradually from the rectum to cecum in serrated lesions as did the occurrence of *BRAF* mutation, CIMP-high status and *MLH1* methylation.

miR-31 is located at 9p21.3 and is reportedly up-regulated in CRCs.[31–35,37] We recently reported an association among miR-31 expression, *BRAF* mutation and poor prognosis involving a large CRC sample ($N = 721$); we also reported that high miR-31 expression is frequently detected in the proximal colon (cecum and ascending and transverse colon) compared to that in the distal colon (the descending and sigmoid colon) and rectum.[38] Because the presence of *BRAF* mutation is tightly associated with CIMP status,[20,44–46] we examined the association between miR-31 expression and CIMP status in serrated lesions. With regard to CRCs, Slattery *et al.* reported that miR-31 was the one of the upregulated miRNAs in patients with CIMP-high status; however, they did not examine *BRAF* mutations.[47] Moreover, no previous study has reported the association between miR-31 expression and CIMP status in premalignant colorectal lesions.

Our current study had some limitations due to its cross-sectional nature and the fact that unknown bias (*i.e.* selection bias) may have confounded the results. Nevertheless, our multivariate regression analysis was adjusted for potential confounders including clinical and molecular features. The results demonstrated that high miR-31 expression is independently associated with *BRAF* status in serrated lesions. In contrast, although we found that miR-31 expression was associated with CIMP-high

Table 2. Epigenetic features, CIMP status, MSI and microRNA-31 expression in serrated lesions according to histopathology

	Histopathology						
		Sessile serrated adenomas (SSAs)			Traditional serrated adenomas (TSAs)		
Molecular features	Hyperplastic polyps (HPs)	SSAs	SSAs withcytological dysplasia	*P*	TSAs	TSAs withhigh-grade dysplasia	*P*
All cases	132	122	10		101	16	
MGMT methylation							
Unmethylated	126 (95%)	113 (93%)	6 (60%)	0.0071	98 (97%)	10 (63%)	<0.0001
Methylayed	6 (4.6%)	9 (7.4%)	4 (40%)		3 (3.0%)	6 (38%)	
MLH1 methylation							
Unmethylated	127 (96%)	102 (84%)	2 (20%)	<0.0001	97 (96%)	16 (100%)	0.27
Methylayed	5 (3.8%)	20 (16%)	8 (80%)		4 (4.0%)	0 (0%)	
CIMP status							
CIMP-low/zero	121 (92%)	76 (62%)	0 (0%)	<0.0001	89 (89%)	4 (25%)	<0.0001
CIMP-high	11 (8.3%)	46 (38%)	10 (100%)		12 (11%)	12 (75%)	
MSI							
MSI-low/MSS	131 (99%)	121 (99%)	6 (60%)	<0.0001	98 (97%)	16 (100%)	0.34
MSI-high	1 (0.8%)	1 (0.8%)	4 (40%)		3 (3.0%)	0 (0%)	
MicroRNA-31							
Q1 (<1.6)	39 (30%)	10 (8.2%)	0 (0%)	0.0079	11 (11%)	3 (19%)	0.23
Q2 (1.6–7.3)	47 (36%)	30 (25%)	0 (0%)		17 (17%)	5 (31%)	
Q3 (7.4–30.2)	27 (20%)	44 (36%)	2 (20%)		33 (33%)	2 (13%)	
Q4 (≥30.2)	19 (14%)	38 (31%)	8 (80%)		40 (40%)	6 (38%)	

Percentage (%) indicates the number of cases with a specific molecular feature according to histopathology. *p*-Values were calculated by chi-square or Fisher's exact test.
Abbreviations: CIMP: CpG island methylator phenotype; HP: hyperplastic polyp; MSI: microsatellite instability; MSS: microsatellite stable; SSA: sessile serrated adenoma; TSA: traditional serrated adenoma.

status in serrated lesions with *BRAF* mutation, the relationship between miR-31 expression and CIMP status did not persist in the cases with wild-type *BRAF*. These results suggested that the association between miR-31 expression and CIMP-high status may have been due to *BRAF* mutation. However, the number of samples of CIMP-high serrated lesions with wild-type *BRAF* was too small ($N = 19$). Moreover, multivariate logistic regression analysis showed that CIMP status was one of the variables associated with miR-31 expression, although no significant association was observed. Therefore, our results imply that epigenetic instability (*i.e.* CIMP-high status) may be related to up-regulation of miR-31 expression. Further functional analysis is needed to clarify the associations between miR-31 expression, *BRAF* mutations and CIMP status in colorectal neoplastic disease.

Accumulating evidence suggests that proximal colon cancers differ from distal cancers in clinical, pathological and molecular features.[18,40,41,47] Yamauchi *et al.* reported that the frequency of CIMP-high, MSI-high and *BRAF* mutation increase gradually along colorectum subsites from the rectum to the ascending colon; these data support the colorectal continuum concept, namely, gradual changes in tumor molecular features, rather than abrupt changes at the splenic flexure (the "Two-colon concept").[20] Colorectal epithelial cells are constantly in contact with bowel contents, which may play a critical role in cellular transformation and tumor development and progression. Bowel contents (*i.e.* food debris and microbiome) and their interactions with host cells may directly cause cellular molecular changes, or alternatively, may influence tumor progression differentially according to molecular features in premalignant cells.[20] In fact, bowel contents gradually change, and this observation may explain why molecular features of a tumor change gradually. Our current data using serrated lesions and non-serrated adenomas seems to be consistent with a previous study[20] because the frequency of *BRAF* mutation, CIMP-high and *MLH1* methylation increased along the bowel from the rectum to the cecum. These results indicate that gradual changes in tumor molecular features already occur at the early stage of colorectal neoplastic disease.

In the current study, we also found that the frequency of high miR-31 expression increased gradually from the rectum to the cecum in serrated lesions. Similar results were observed in non-serrated adenomas and CRCs. These results show that miR-31 may be a molecule that supports the

colorectal continuum concept. To the best of our knowledge, no previous reports have described a specific miRNA associated with this concept. Thus, our data on miR-31 and other molecular features indicate that future studies on colorectal tumors should include information on detailed tumor locations (beyond the proximal colon, distal colon and rectum).

Various authors have reported that SSAs with cytological dysplasia have genetic and epigenetic abnormalities and are at a high risk of progression to CRCs.[4,9,25,27,46] A loss of staining for MLH1 (due to *MLH1* methylation) leads to MSI, and repeat tract mutation in genes such as *TGFβRII* is restricted to the lesions with cytological dysplasia in SSAs.[25,26,48–50] In addition, Dhir *et al.* recently reported that there was a progressive increase in the methylation frequencies of genes from HPs to SSAs to SSAs with cytological dysplasia.[51] Our current data showed that the frequency of high miR-31 expression, *MLH1* and *MGMT* methylation and CIMP-high in SSAs with cytological dysplasia is much higher than in SSAs without. Thus not only accumulating epigenetic alterations but also miR-31 expression may play a role in SSA progression. In contrast, TSAs are much less common than SSAs; therefore, there fewer data is available on their molecular profile.[4,24] TSAs typically do not show *MLH1* methylation or develop into MSI-high CRCs, but they do commonly have *MGMT* methylation.[4,24,25] In addition, the key molecule of the TSA pathway progression remains largely unknown. In the current study, no significant differences in miR-31 expression or *MLH1* methylation were found between TSAs with and without HGD, whereas the frequency of high CIMP status and *MGMT* methylation was much higher in TSAs with HGD than in TSAs without. These results suggest that the molecule controlling serrated lesion progression may distinguish TSAs from SSAs.

In conclusion, miR-31 expression was associated with CIMP-high status in serrated lesions with *BRAF* mutation. Our data also suggest that miR-31 may play an important role in SSA evolution. Moreover, we found that not only *BRAF* mutation and CIMP status but also miR-31 may be a key molecule that supports the colorectal continuum concept. These novel data will improve our understanding of details of the colorectal serrated pathway and may lead to the establishment of a new therapeutic target or a theranostic procedure in some CRC types.

Acknowledgements

The authors thank the pathology departments of Sapporo Medical University Hospital and Keiyukai Sapporo Hospital for providing the tissue specimens. They also thank Enago (www.enago.jp) for the English language review.

Author Contributions

Study concept and design: KN

Data acquisition: MI, KM, HI, TN, SY, MF

Data analysis and interpretation: EY, KN, MN, YS, YA, TT, RM, YB

Drafting of the manuscript: MI, KN

Critical revision of the manuscript for important intellectual content: KN, HY, YS

Statistical analysis: KN, MN

Material support: HT, TT,

Study supervision: KN, HS, HY, KI, YS

Final approval of manuscript: all authors.

References

1. Edelstein DL, Axilbund JE, Hylind LM, et al. Serrated polyposis: rapid and relentless development of colorectal neoplasia. *Gut* 2013;62:404–8.
2. Spring KJ, Zhao ZZ, Karamatic R, et al. High prevalence of sessile serrated adenomas with BRAF mutations: a prospective study of patients undergoing colonoscopy. *Gastroenterology* 2006;131:1400–7.
3. Rosty C, Buchanan DD, Walsh MD, et al. Phenotype and polyp landscape in serrated polyposis syndrome: a series of 100 patients from genetics clinics. *Am J Surg Pathol* 2012;36:876–82.
4. Rex DK, Ahnen DJ, Baron JA, et al. Serrated lesions of the colorectum: review and recommendations from an expert panel. *Am J Gastroenterol* 2012;107:1315–29; quiz 14, 30.
5. Burnett-Hartman AN, Newcomb PA, Potter JD, et al. Genomic aberrations occurring in subsets of serrated colorectal lesions but not conventional adenomas. *Cancer Res* 2013;73:2863–72.
6. Carr NJ, Mahajan H, Tan KL, et al. Serrated and non-serrated polyps of the colorectum: their prevalence in an unselected case series and correlation of BRAF mutation analysis with the diagnosis of sessile serrated adenoma. *J Clin Pathol* 2009;62:516–8.
7. Yachida S, Mudali S, Martin SA, et al. Beta-catenin nuclear labeling is a common feature of sessile serrated adenomas and correlates with early neoplastic progression after BRAF activation. *Am J Surg Pathol* 2009;33:1823–32.
8. Kim KM, Lee EJ, Kim YH, et al. KRAS mutations in traditional serrated adenomas from Korea herald an aggressive phenotype. *Am J Surg Pathol* 2010;34:667–75.
9. Fujita K, Yamamoto H, Matsumoto T, et al. Sessile serrated adenoma with early neoplastic progression: a clinicopathologic and molecular study. *Am J Surg Pathol* 2011;35:295–304.
10. Han Y, Zhou ZY. Clinical features and molecular alterations of traditional serrated adenoma in sporadic colorectal carcinogenesis. *J Dig Dis* 2011; 12:193–8.
11. Fu B, Yachida S, Morgan R, et al. Clinicopathologic and genetic characterization of traditional serrated adenomas of the colon. *Am J Clin Pathol* 2012;138:356–66.
12. Mohammadi M, Kristensen MH, Nielsen HJ, et al. Qualities of sessile serrated adenoma/polyp/lesion and its borderline variant in the context of synchronous colorectal carcinoma. *J Clin Pathol* 2012;65:924–7.
13. Kaji E, Uraoka T, Kato J, et al. Externalization of saw-tooth architecture in small serrated polyps implies the presence of methylation of IGFBP7. *Dig Dis Sci* 2012;57:1261–70.
14. Hiraoka S, Kato J, Fujiki S, et al. The presence of large serrated polyps increases risk for colorectal cancer. *Gastroenterology* 2010;139:1503–10, 10 e1–3.
15. Gonzalo DH, Lai KK, Shadrach B, et al. Gene expression profiling of serrated polyps identifies annexin A10 as a marker of a sessile serrated adenoma/polyp. *J Pathol* 2013;230:420–9.
16. Gaiser T, Meinhardt S, Hirsch D, et al. Molecular patterns in the evolution of serrated lesion of the colorectum. *Int J Cancer* 2013;132:1800–10.
17. Whitehall VL, Rickman C, Bond CE, et al. Oncogenic PIK3CA mutations in colorectal cancers and polyps. *Int J Cancer* 2012;131:813–20.
18. Toyota M, Ahuja N, Ohe-Toyota M, et al. CpG island methylator phenotype in colorectal cancer. *Proc Natl Acad Sci USA* 1999;96:8681–6.
19. Weisenberger DJ, Siegmund KD, Campan M, et al. CpG island methylator phenotype underlies sporadic microsatellite instability and is tightly associated with BRAF mutation in colorectal cancer. *Nat Genet* 2006;38:787–93.
20. Yamauchi M, Morikawa T, Kuchiba A, et al. Assessment of colorectal cancer molecular features along bowel subsites challenges the conception of distinct dichotomy of proximal versus distal colorectum. *Gut* 2012;61:847–54.

21. Nosho K, Irahara N, Shima K, et al. Comprehensive biostatistical analysis of CpG island methylator phenotype in colorectal cancer using a large population-based sample. *PLoS One* 2008;3:e3698.
22. Network TCGA. Comprehensive molecular characterization of human colon and rectal cancer. *Nature* 2012;487:330–7.
23. Donehower LA, Creighton CJ, Schultz N, et al. MLH1-silenced and non-silenced subgroups of hypermutated colorectal carcinomas have distinct mutational landscapes. *J Pathol* 2013;229:99–110.
24. Leggett B, Whitehall V. Role of the serrated pathway in colorectal cancer pathogenesis. *Gastroenterology* 2010;138:2088–100.
25. Bettington M, Walker N, Clouston A, et al. The serrated pathway to colorectal carcinoma: current concepts and challenges. *Histopathology* 2013;62:367–86.
26. Goldstein NS. Small colonic microsatellite unstable adenocarcinomas and high-grade epithelial dysplasias in sessile serrated adenoma polypectomy specimens: a study of eight cases. *Am J Clin Pathol* 2006;125:132–45.
27. Rosty C, Hewett DG, Brown IS, et al. Serrated polyps of the large intestine: current understanding of diagnosis, pathogenesis, and clinical management. *J Gastroenterol* 2013;48:287–302.
28. Kriegl L, Neumann J, Vieth M, et al. Up and downregulation of p16(Ink4a) expression in BRAF-mutated polyps/adenomas indicates a senescence barrier in the serrated route to colon cancer. *Mod Pathol* 2011;24:1015–22.
29. Garcia-Solano J, Conesa-Zamora P, Carbonell P, et al. Colorectal serrated adenocarcinoma shows a different profile of oncogene mutations, MSI status and DNA repair protein expression compared to conventional and sporadic MSI-H carcinomas. *Int J Cancer* 2012;131:1790–9.
30. Conesa-Zamora P, Garcia-Solano J, Garcia-Garcia F, et al. Expression profiling shows differential molecular pathways and provides potential new diagnostic biomarkers for colorectal serrated adenocarcinoma. *Int J Cancer* 2013;132:297–307.
31. Schee K, Boye K, Abrahamsen TW, et al. Clinical relevance of microRNA miR-21, miR-31, miR-92a, miR-101, miR-106a and miR-145 in colorectal cancer. *BMC Cancer* 2012;12:505.
32. Slaby O, Svoboda M, Fabian P, et al. Altered expression of miR-21, miR-31, miR-143 and miR-145 is related to clinicopathologic features of colorectal cancer. *Oncology* 2007;72:397–402.
33. Cekaite L, Rantala JK, Bruun J, et al. MiR-9, -31, and -182 deregulation promote proliferation and tumor cell survival in colon cancer. *Neoplasia* 2012;14:868–79.
34. Chang KH, Miller N, Kheirelseid EA, et al. MicroRNA signature analysis in colorectal cancer: identification of expression profiles in stage II tumors associated with aggressive disease. *Int J Colorectal Dis* 2011;26:1415–22.
35. Sarver AL, French AJ, Borralho PM, et al. Human colon cancer profiles show differential microRNA expression depending on mismatch repair status and are characteristic of undifferentiated proliferative states. *BMC Cancer* 2009;9:401.
36. Hur K, Toiyama Y, Takahashi M, et al. MicroRNA-200c modulates epithelial-to-mesenchymal transition (EMT) in human colorectal cancer metastasis. *Gut* 2013;62:1315–26.
37. Sun D, Yu F, Ma Y, et al. MicroRNA-31 activates the RAS pathway and functions as an oncogenic MicroRNA in human colorectal cancer by repressing RAS p21 GTPase activating protein 1 (RASA1). *J Biol Chem* 2013;288:9508–18.
38. Nosho K, Igarashi H, Nojima M, et al. Association of microRNA-31 with BRAF mutation, colorectal cancer survival and serrated pathway. *Carcinogenesis* 2014;35:776–83.
39. Iacopetta B. Are there two sides to colorectal cancer? *Int J Cancer* 2002;101:403–8.
40. Papagiorgis P. Colorectal cancer: dichotomous or continuum model? Perhaps, a combination of both. *Gut* 2013;62:1519–20.
41. Yamauchi M, Lochhead P, Morikawa T, et al. Colorectal cancer: a tale of two sides or a continuum? *Gut* 2012;61:794–7.
42. Bosman FT, World Health Organization, International Agency for Research on Cancer. WHO classification of tumours of the digestive system, 4th edn. Lyon: International Agency for Research on Cancer, 2010.
43. Liao X, Lochhead P, Nishihara R, et al. Aspirin use, tumor PIK3CA mutation, and colorectal-cancer survival. *N Engl J Med* 2012;367:1596–606.
44. Nosho K, Yamamoto H, Takahashi T, et al. Correlation of laterally spreading type and JC virus with methylator phenotype status in colorectal adenoma. *Hum Pathol* 2008;39:767–75.
45. Nosho K, Yamamoto H, Takahashi T, et al. Genetic and epigenetic profiling in early colorectal tumors and prediction of invasive potential in pT1 (early invasive) colorectal cancers. *Carcinogenesis* 2007;28:1364–70.
46. Yamamoto E, Suzuki H, Yamano HO, et al. Molecular dissection of premalignant colorectal lesions reveals early onset of the CpG island methylator phenotype. *Am J Pathol* 2012;181:1847–61.
47. Slattery ML, Wolff E, Hoffman MD, et al. MicroRNAs and colon and rectal cancer: differential expression by tumor location and subtype. *Genes, chromosomes & cancer* 2011;50:196–206.
48. Ricciardiello L, Goel A, Mantovani V, et al. Frequent loss of hMLH1 by promoter hypermethylation leads to microsatellite instability in adenomatous polyps of patients with a single first-degree member affected by colon cancer. *Cancer Res* 2003;63:787–92.
49. Cunningham JM, Christensen ER, Tester DJ, et al. Hypermethylation of the hMLH1 promoter in colon cancer with microsatellite instability. *Cancer Res* 1998;58:3455–60.
50. Sheridan TB, Fenton H, Lewin MR, et al. Sessile serrated adenomas with low- and high-grade dysplasia and early carcinomas: an immunohistochemical study of serrated lesions "caught in the act". *Am J Clin Pathol* 2006;126:564–71.
51. Dhir M, Yachida S, van Neste L, et al. Sessile serrated adenomas and classical adenomas: an epigenetic perspective on premalignant neoplastic lesions of the gastrointestinal tract. *Int J Cancer* 2011;129:1889–98.

Tumor Biol. (2014) 35:973–985
DOI 10.1007/s13277-013-1131-2

RESEARCH ARTICLE

The effect of IGF-I receptor blockade for human esophageal squamous cell carcinoma and adenocarcinoma

Yasushi Adachi · Hirokazu Ohashi · Arisa Imsumran · Hiroyuki Yamamoto · Yasutaka Matsunaga · Hiroaki Taniguchi · Katsuhiko Nosho · Hiromu Suzuki · Yasushi Sasaki · Yoshiaki Arimura · David P Carbone · Kohzoh Imai · Yasuhisa Shinomura

Received: 1 August 2013 / Accepted: 21 August 2013 / Published online: 13 September 2013

Abstract Insulin-like growth factor-I receptor (IGF-IR) signaling is required for carcinogenicity and tumor development, and this pathway has not been well studied in human esophageal carcinomas. Esophageal cancer is one of the human cancers with the worst prognosis and has two main histologies: squamous cell carcinomas (ESCC) and adenocarcinoma (EAC). Previously, we have reported that detection of the IGF axis may be useful for the prediction of recurrence and poor prognosis of ESCC. We have also shown the successful therapy for several gastrointestinal cancers using recombinant adenoviruses expressing dominant negative IGF-IR (ad-IGF-IR/dn). The aim of this study is to develop potential targeted therapeutics to IGF-IR and to assess the effect of IGF-IR blockade in both of these types of esophageal cancer. We determined immunohistochemical expression of IGF-IR in a tissue microarray. We then assessed the effect of IGF-IR blockade on signal transduction, proliferation, apoptosis, and motility. Ad-IGF-IR/dn, a tyrosine kinase inhibitor, BMS-536924, and adenovirus expressing shRNA for IGF-IR were used. IGF-IR expression was common in both tumor types but not in normal tissues. IGF-IR was detected in metastatic sites at similar levels compared to the primary site. IGF-IR inhibition suppressed proliferation and colony formation in both cancers. IGF-IR blockades up-regulated both stress- and chemotherapy-induced apoptosis and reduced migration. Although IGF-IR/dn blocked ligand-induced activation of Akt-1 mainly, BMS-536924 effectively blocked both activation of Akt and MAPK. The IGF axis might play a key role in tumor progression of esophageal carcinomas. The IGF-IR targeting strategies might thus be useful anticancer therapeutics for human esophageal malignancies.

Keywords Dominant negative · EAC · ESCC · IGF-IR · TKI

Abbreviations

ad-IGF-IR/482st	Adenovirus expressing IGF-IR /482st
ad-IGF-IR/950st	Adenovirus expressing IGF-IR/950st
ad-shIG F-IR	Adenovirus expressing short-hairpin IGF-IR
des(1–3)IGF-I	NH_2 terminally truncated IGF-I
dn	Dominant negative
EAC	Esophageal adenocarcinoma
ESCC	Esophageal squamous cell carcinoma
ERK	Extracellular signal-regulated kinase
IGF	Insulin-like growth factor
IGFBP	IGF binding protein
IGF-IR	IGF-I receptor
IGF-IR/482st	Truncated IGF-IR of 482 amino acid long

Yasushi Adachi, Hirokazu Ohashi, and Arisa Imsumran contributed equally to this work.

Y. Adachi (✉) · H. Ohashi · A. Imsumran · H. Yamamoto · Y. Matsunaga · K. Nosho · H. Suzuki · Y. Sasaki · Y. Arimura · K. Imai · Y. Shinomura
First Department of Internal Medicine, Sapporo Medical University, S-1, W-16, Chuo-ku, Sapporo 060-8543, Japan
e-mail: yadachi@sapmed.ac.jp

H. Taniguchi · K. Imai
The Institute of Medical Science, The University of Tokyo, Tokyo, Japan

D. P. Carbone
James Thoracic Center, The Ohio State University, Columbus, OH, USA

IGF-IR/950st	Truncated IGF-IR of 950 amino acid long
IGF-IR/dn	Dominant negative form of IGF-IR
InsR	Insulin receptor
mAb	Monoclonal antibody
PI3-K	Phosphatidylinositide 3-kinase
TKI	Tyrosine kinase inhibitor

Introduction

Esophageal cancer is one of the cancers with the worse prognosis worldwide [1]. At the time of diagnosis, more than half of patients have either unresectable tumors or metastatic ones. Even after a curative-intent surgical operation, the 5-year survival is still limited [2], and the therapy for unresectable esophageal carcinomas is typically minimally effective. Therefore, we must aim to seek new therapeutic options for this disease. The main types of human esophageal tumor are squamous cell carcinoma (ESCC) and adenocarcinoma (EAC).

Recently, advances in molecular research have brought new therapeutic strategies, including small molecule tyrosine kinase inhibitors (TKI) and monoclonal antibodies (mAb), into clinical testing. One group of new targets is the tyrosine kinase receptors. The insulin-like growth factor (IGF) family is a promising candidate [3, 4]. Agents targeting the IGF-I receptor (IGF-IR) pathway are moving into the clinic. Toward that end, we have studied this pathway in esophageal cancers.

IGF-IR is a heterotetramer of two α- and two β-chains [5]. Binding of the ligands IGF-I and IGF-II to IGF-IR causes receptor autophosphorylation and activates multiple signaling pathways, including ras/extracellular signal-regulated kinase (ERK) and the phosphatidylinositide 3-kinase (PI3-K)/Akt-1 axes [6]. Activation of IGF-IR is regulated by multiple factors, including IGF binding proteins (IGFBP) and IGF-2 receptor [7–9]. Elevation of serum IGF-I increases the risk of developing several cancers [10], and IGF-IR is essential for both malignant transformation and progression [3, 4]. Reduction of IGF-IR can induce apoptosis in tumors but produces only growth slowing in untransformed cells, suggesting that it might be an excellent target for therapeutic intervention [3]. IGF-IR knockout mice are viable (though physically small), indicating that relatively normal development and differentiation can occur in its absence [11]. These findings suggest a potential basis for tumor selectivity in therapeutic applications.

Human esophageal epithelial cells express IGF-IR, and IGF-I can stimulate both DNA synthesis and proliferation in these cells [12–14]. Salivary IGF-I continuously bathes the esophageal lumen and is in a free form (not bound to IGFBP, unlike the serum pool), which could enhance its binding ability to receptors on the esophageal mucosal cells [15]. These data indicate that the IGF/receptor may play important roles in homeostasis and esophageal premalignancy [14].

Both IGF-IR and IGFs are overexpressed in esophageal cancer tissues compared to normal ones [16–18]. In addition, IGFBP3 and an IGF-IR antibody suppress cancer cell proliferation [19, 20]. However, the role of the IGF axis in esophageal cancer has not been adequately studied. We reported previously that expression of IGF-IR and IGF-II were detected in 60 and 50% of ESCC, respectively, and were associated with invasion depth, metastasis, advanced tumor stage, and recurrence [21]. Patients with ESCC expressing both IGF-IR and IGF-II had a significantly shorter survival rate than those expressing either alone or neither in both single and multivariate analysis. Dominant negative for IGF-IR (IGF-IR/dn) suppressed proliferation and up-regulating chemotherapy-induced apoptosis through blocking ligand-induced Akt activation in an ESCC cell line, TE-1 [21].

In addition, there is a strong positive association between visceral obesity (metabolic syndrome) and risk of EAC, and the IGF axis is speculated to relate to both obesity and EAC [22]. IGF-IR expression in resected EAC was significantly higher in viscerally obese patients than in those of normal weight. Disease-specific survival was longer in patients with IGF-IR-negative EAC than in those with IGF-IR-positive tumors [23]. Thus, there are several lines of evidence that the IGF axis may play an important role in EAC.

There are several possible approaches to blocking IGF-IR signaling with therapeutic intent [24], including blocking the ligand or receptor using mAbs [25, 26] or TKIs [27, 28]. All of these are complicated by the high homology of this receptor to the insulin receptor (InsR). An approach that is intrinsically specific for IGF-IR is to use dominant negative or soluble IGF-IR receptor approaches to specifically inhibit the function of the wild-type receptor [29, 30]. We have constructed two different adenoviruses expressing IGF-IR/dn (ad-IGF-IR/dn) [31–34]. Ad-IGF-IR/482st encodes a truncated extracellular domain of IGF-IR (without the transmembrane domain) and thus produces a secreted protein that affects neighboring cells in addition to the transduced cells (a bystander effect). Another ad-IGF-IR/950st encodes a receptor that lacks the tyrosine kinase domain and thus remains on the membrane of the transduced cells to form non-functional receptor complexes. We have reported that ad-IGF-IR/dn may be a useful therapeutic strategy against several gastrointestinal tumors [21, 31, 32, 34, 35]. We have also reported that the adenoviral vector-based approach to express a short-hairpin inhibitory RNA of IGF-IR (ad-shIGF-IR) induced effective IGF-IR silencing in gastrointestinal cancers as manifested by effective blockade of the downstream pathway of IGF-IR and antitumor effects [36]. A dual targeting TKI for IGF-IR/InsR, BMS-536924, may have an advantage compared to a single targeting TKI,

as transformed cells can also use insulin receptor activation of similar signaling pathways for proliferation in addition to IGFR signals [35, 37].

In order to evaluate the expression of IGF-IR in EAC and in metastatic sites of ESCC, we analyzed an esophageal cancer tissue microarray immunohistochemically. To assess IGF-IR blockade for both esophageal cancers, histologies ESCC and EAC, we used several strategies including IGF-IR/dns, shIGF-IR, and BMS-536924.

Methods

Materials, cell lines, and recombinant adenovirus vectors

Anti-Akt1(c-20), anti-ERK1(K-23), anti-phospho-ERK1(E-4), ant-IGF-I(G-17), and anti-IGF-IRβ(2C8) were purchased from Santa Cruz Biotechnology (Santa Cruz, CA, USA) and anti-phospho-Akt(Ser473) was from Cell-Signaling Technology (Beverly, MA, USA). Anti-IGF-IR(Ab-4) was from Oncogene Research Products (Cambridge, MA, USA) and anti-IGF-II was from Peninsula Laboratories (San Carlos, CA, USA). PI3-K inhibitors, wortmannin and LY294002, p38-MAPK inhibitor SB203580, cisplatin (CDDP), and 5-fluorouracil (5-FU) were purchased from Sigma (St. Louis, MO, USA), and MEK1 inhibitor PD98059 was from Cell Signaling. Recombinant human IGF-I and IGF-II were purchased from R&D systems (Minneapolis, MN, USA) and des(1–3)IGF-I from GroPep (Adelaide, Australia). All human esophageal cancer cell lines (Fig. 1) were obtained from the Japanese Cancer Collection of Research Bioresources Cell Bank (Tokyo, Japan), Riken Bioresource Center Cell Bank (Tsukuba, Japan), and European Collection of Cell Cultures (Salisbury, UK). Cells were passaged in RPMI1640 and DMEM, both with 10% fetal bovine serum.

Recombinant adenoviruses expressing IGF-IR/dn (482 and 950 amino acids long, IGF-IR/482st and IGF-IR/950st, Ad-IGF-IR/482st and Ad-IGF-IR/950st, respectively) were generated as described previously by homologous recombination [31]. Recombinant adenovirus vectors expressing shIGF-IR (ad-shIGF-IR) were generated as described previously [38]. An adenovirus expressing β-galactosidase was used as a control (ad-LacZ). Scrambled shRNA adenovirus (ad-Scr) is another control that has a short hairpin sequence but no specific target, also as described previously.

BMS-536924 was kindly provided by Bristol-Myers Squibb (New York, NY, USA). Stock solution was prepared in DMSO and stored at −20°C.

Immunohistochemical analysis

The paraffin-embedded esophageal tissue microarray (ES208) was purchased from US Biomax (Rockville, MD, USA). After deparaffinization, endogenous peroxidase activity was blocked. Antibodies were applied after blocking with normal goat serum. Sections were incubated with the anti-rabbit secondary antibody (Santa Cruz Biotechnology) and a strep tavidin-HRP followed by exposure to the diaminobenzidine tetrahydrochloride substrate (Dako). The sections were counterstained in Mayer's hematoxylin and mounted. Immunostaining signals were scored by two independent observers. Semiquantitative scores were given as the score of the percentage of positive cells plus the score of the staining intensity. The scoring criteria of the percentage of positive cells were as follows: score 0, 0–5% positive cancer cells; score 1, 6–25%; score 2, 26–50%; score 3, 51–75%; score 4, 76–100% positive. The intensity score was given as follows: score 0, no staining; score 1, weak/equivocal; score 2, moderate; score 3,

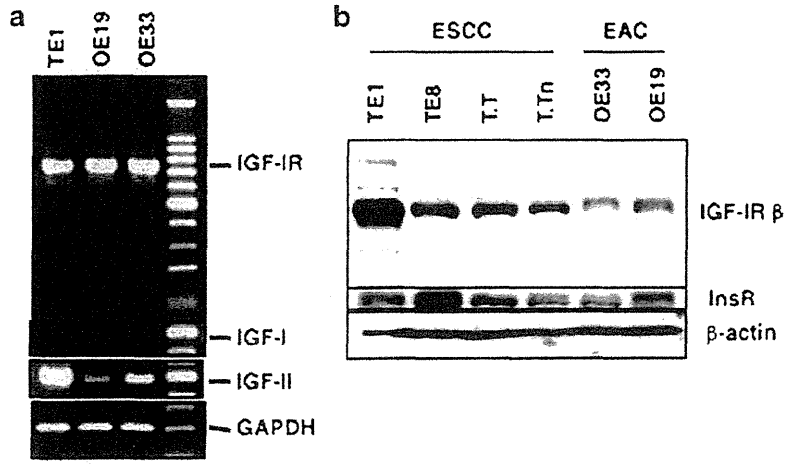

Fig. 1 The expressions of IGF-axis in esophageal carcinoma cell lines. **a** RT-PCR revealed that three cells express mRNAs of IGF-II and IGF-IR but not IGF-I. **b** Western blotting showed that two EAC and four ESCC cells express both IGF-IR and InsR

strong staining. The final scores were from 0 to 7 and four or more were considered positive.

Reverse transcription PCR

Total RNA from cells was isolated by the acid guanidinium thiocyanate–phenol–chloroform method. Primer sets for the amplification of IGF-I cDNA sequences were 5′-CACTGT CACTGCTAAATTCA-3′ and 5′-CTGTGGGCTTGTTGAAA TAA-3′ [39]. Primers for IGF-II cDNA were 5′-AGTCGATGC TGGTGCTTCTCA-3′ and 5′-GTGGGCGGGGTCTTGG GTGGGTAG-3′ [40]. Primers for IGF-IR were 5′-ATTGAG GAGGTCACAGAGAAC-3′ and 5′-TTCATATCCTGTTTT GGCCTG-3′ [40]. Randomly primed cDNAs were prepared from 1 mg of total RNA by M-MLV reverse transcriptase (Takara, Japan) and amplified by PCR. For amplification of these sequences, 35 cycles of PCR was programmed as follows: 94°C, 30 s; 60°C, 30 s; 72°C, 30 s.

Western blotting

Cells were cultured in serum-free medium for 24 h and then stimulated with 20 ng/ml IGF-I or 10 nM insulin. Cell lysates were prepared as described previously [31]. Equal aliquots of lysate (100 μg) were separated by 4–20% SDS-PAGE and immunoblotted onto polyvinylidene Hybond-P membrane (Amersham, Arlington Heights, IL, USA). Analysis was performed using the indicated antibodies, and bands were visualized by ECL (Amersham).

Assessment of the effect on in vitro cell growth

Tumor cells were grown to 70% confluence in six-well plates and infected with adenovirus. The number of cells was then assayed by Trypan blue staining.

Four thousand cells were seeded into the wells of a 96-well plate, and each was infected with adenovirus or control. Cell growth was measured using WST-1 reagent (Roche, Basel, Switzerland) as described previously [21].

In vitro tumorigenicity

Anchorage-independent growth was assessed by soft agar clonogenicity assays. Briefly, cells were detached and plated in 0.2% agarose with 1% underlay (2×10^4 cells/5-cm dish). After 1 week, media were added over the soft agar. The medium overlay was changed after 1 week. Colonies greater than 125 μm were counted after 3 weeks using a calibrated graticule.

Colony forming activity was assessed by plating 3×10^3 per plate on 60-mm culture dishes and incubated for 24 h. The cells were then treated with BMS-536924 and were incubated for 14 days. After air-drying, cells were fixed with methanol and stained with Giemsa solution. Colonies containing 50 cells or more were counted.

Measurement of apoptosis

The DNA fragmentation assay was performed as follows: low molecular weight DNA was extracted with 0.5% Triton X-100, 10 nM EDTA, and 10 mM Tris–HCl, pH 7.4, treated with 400 μg/ml RNase A and then proteinase K for 1 h at 37°C, ethanol-precipitated, and subjected to 1% agarose gel electrophoresis. The gels were stained with 1 μg/ml ethidium bromide. Early apoptosis was quantified by staining with Annexin-V-FITC according to the manufacturer's protocol (BD Biosciences) and measured by flow cytometry. Cells undergoing apoptosis showed an increase in Annexin-V binding but excluded propidium iodide. TUNEL assays were performed with in situ apoptosis detection kit (Takara) following the manufacturer's protocol. Caspase-3 colorimetric protease assay was performed following the manufacturer's protocol (Caspase-3 Colorimetric Protease Assay Kit; MBL). In brief, 3×10^6 cells were lysed in 100 μl of chilled cell lysis buffer, and total cell lysates (100 μg) were incubated with 4 mM VETD-pNA Substrate (200 μM final concentration) at 37°C for 1 h. Caspase-3 activity was measured by colorimetric reaction at 405 nm.

First, cancer cells infected with Ad-IGF-IR/dns or Ad-LacZ were induced with 10 mJ/cm^2 UV light. To assess the efficacy of IGF-IR/dn on chemotherapy-induced apoptosis, tumor cells were treated for 24 h with 1 mM 5-FU or 50 μM cisplatin.

Migration assay

Wounding assays were performed using a modification of the procedure described by Pennisi et al. [41]. Briefly, six-well chambers were prepared by scratching registration marks onto the slide surface. TE1 cells (infected with adenoviruses) were plated, grown normally for 48 h, and starved overnight. Cells were cut with a cell scraper, and five images were captured

Table 1 Summary of immunohistochemical expression of IGF-IR

	IGF-IR (+)		
Normal esophageal mucosa	0/7	0%	
Esophageal carcinoma	31/57	54%	$p = 0.0111$ (Fisher)
	IGF-IR (+)		
Squamous cell carcinoma	23/34	68%	
Primary sites	15/23	65%	
Metastasized sites	8/11	73%	
Lymph node	6/9	67%	
Skin	2/2	100%	
Adenocarcinoma	8/22	36%	
Adenosquamous carcinoma	0/1	0%	

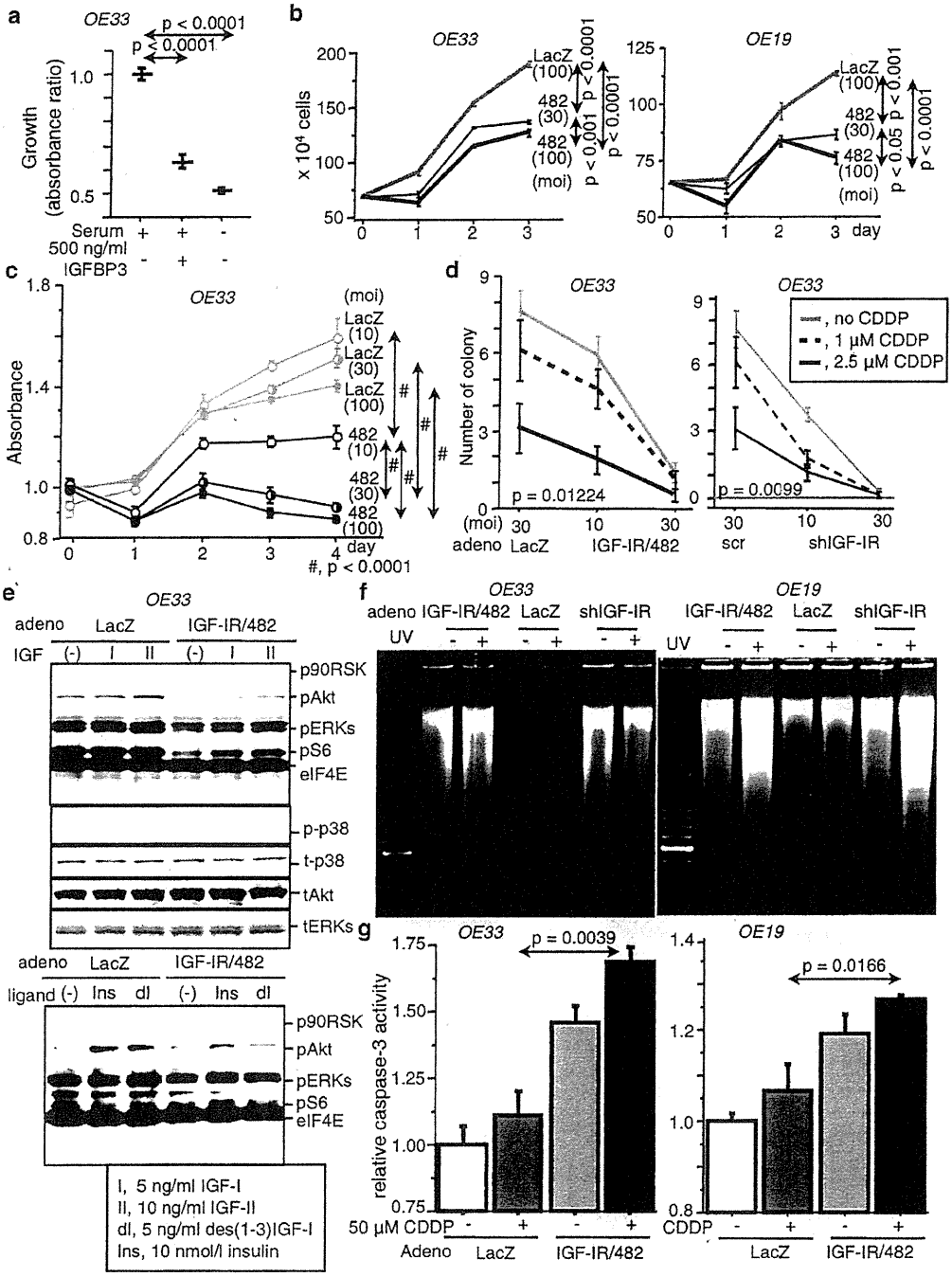

Fig. 2 The effect of IGF-IR on EAC cells. **a** WST-1 assay showed cell growth of OE33, 48 h of culture with/without IGFBP3. **b** Trypan blue assay showed the number of viable cells. **c** WST-1 assay revealed cell proliferation of adenoviruses-infected OE33. **d** Colony formation assays showed the effect of IGF-IR/dn and cisplatin on colony formation. **e** OE33 was stimulated for 5 min with ligands in serum-free medium. Western blotting showed signal transduction. **f** DNA fragmentation assay detected UV-induced apoptosis. **g** Cells were treated for 24 h with cisplatin. Then, caspase-3 assays were performed

along the cut surface on an Olympus IX-71S1F-2 microscope (Tokyo, Japan) using a ×20 objective. Additional images were captured 24 h later. For each experiment, the number of migrating cells was counted by two independent observers [41].

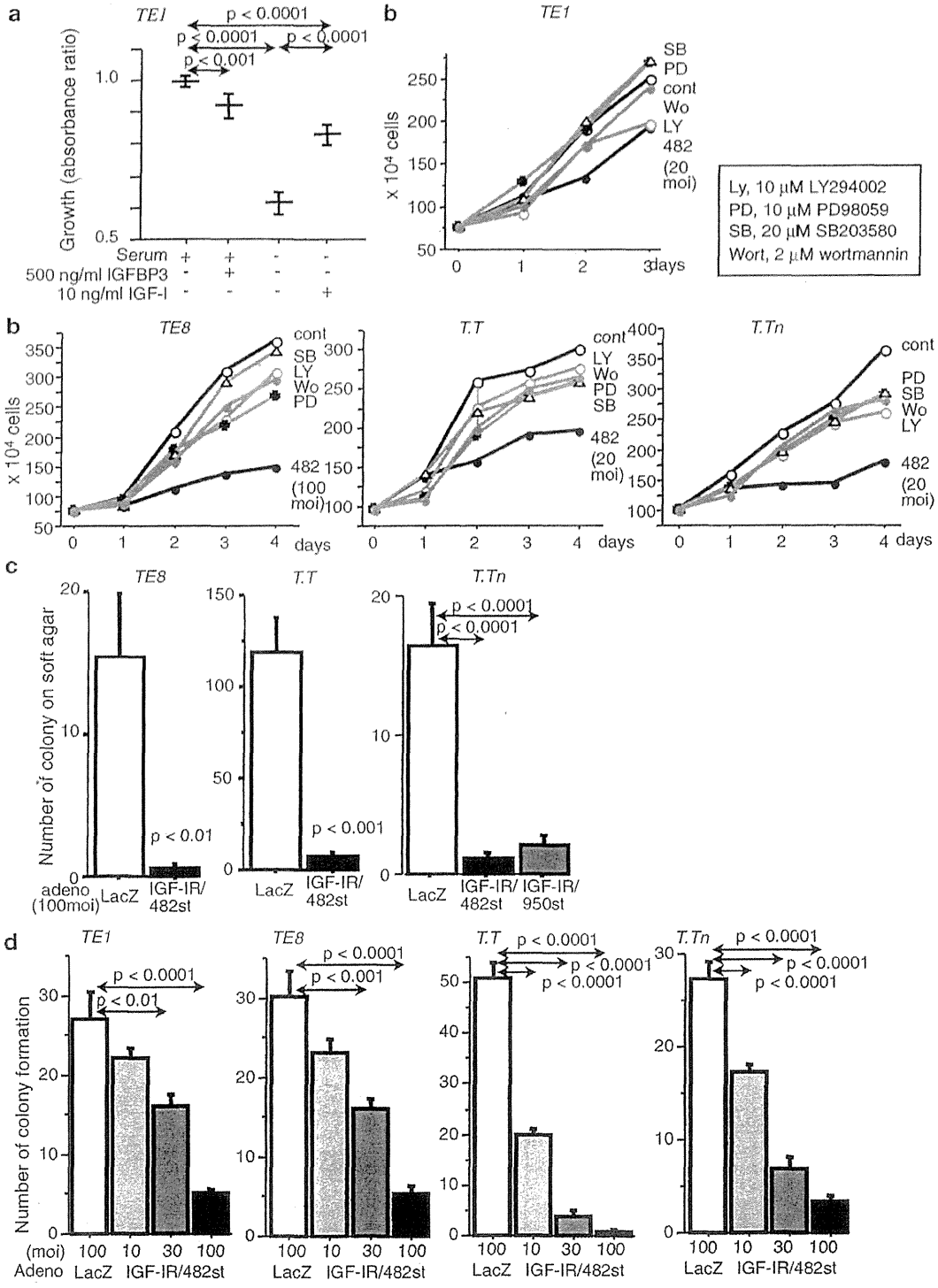

Fig. 3 The effect of IGF-IR on the growth of ESCC. **a** WST-1 assay showed cell growth after 48 h of culture. **b** Trypan blue assay showed the viable cell number of ESCC cells with several inhibitors or IGF-IR/482st. **c** Soft agar assays detected that ad-IGF-IR/dns blocked colony formation. **d** Colony formation assay showed the effect of IGF-IR/482st on colony number

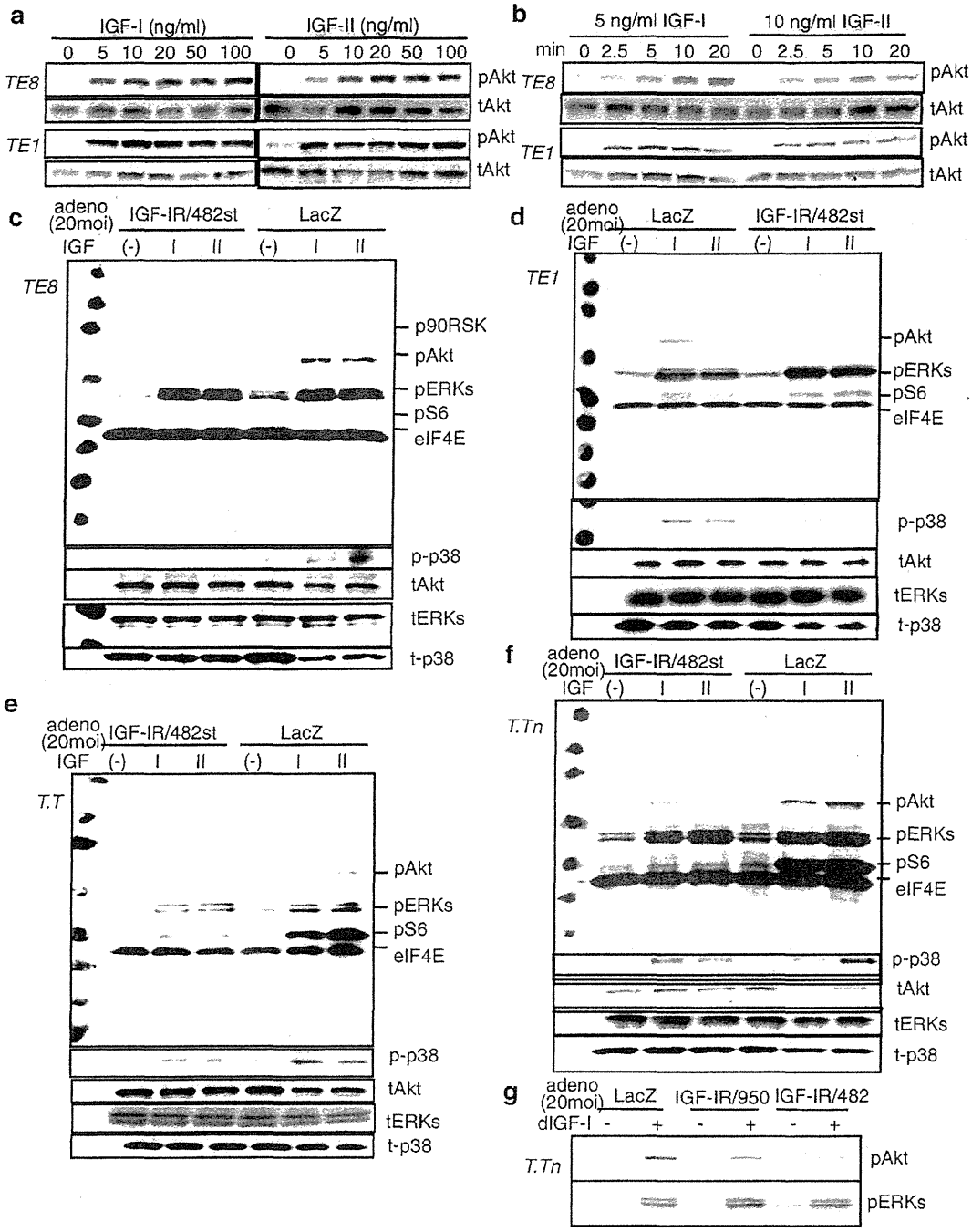

Fig. 4 The down-stream signals from IGF-IR by Western blotting. **a** Both TE8 and TE1 cells were stimulated for 5 min with IGFs, and then whole cell lysates were extracted. **b** Both cells were stimulated from 0 to 20 min with IGFs. **c–f** Four cell lines infected with adenoviruses were stimulated for 5 min with IGFs. **g** Adenoviruses-infected T.Tn cells were stimulated for 5 min with 5 ng/ml des(1–3)IGF-I

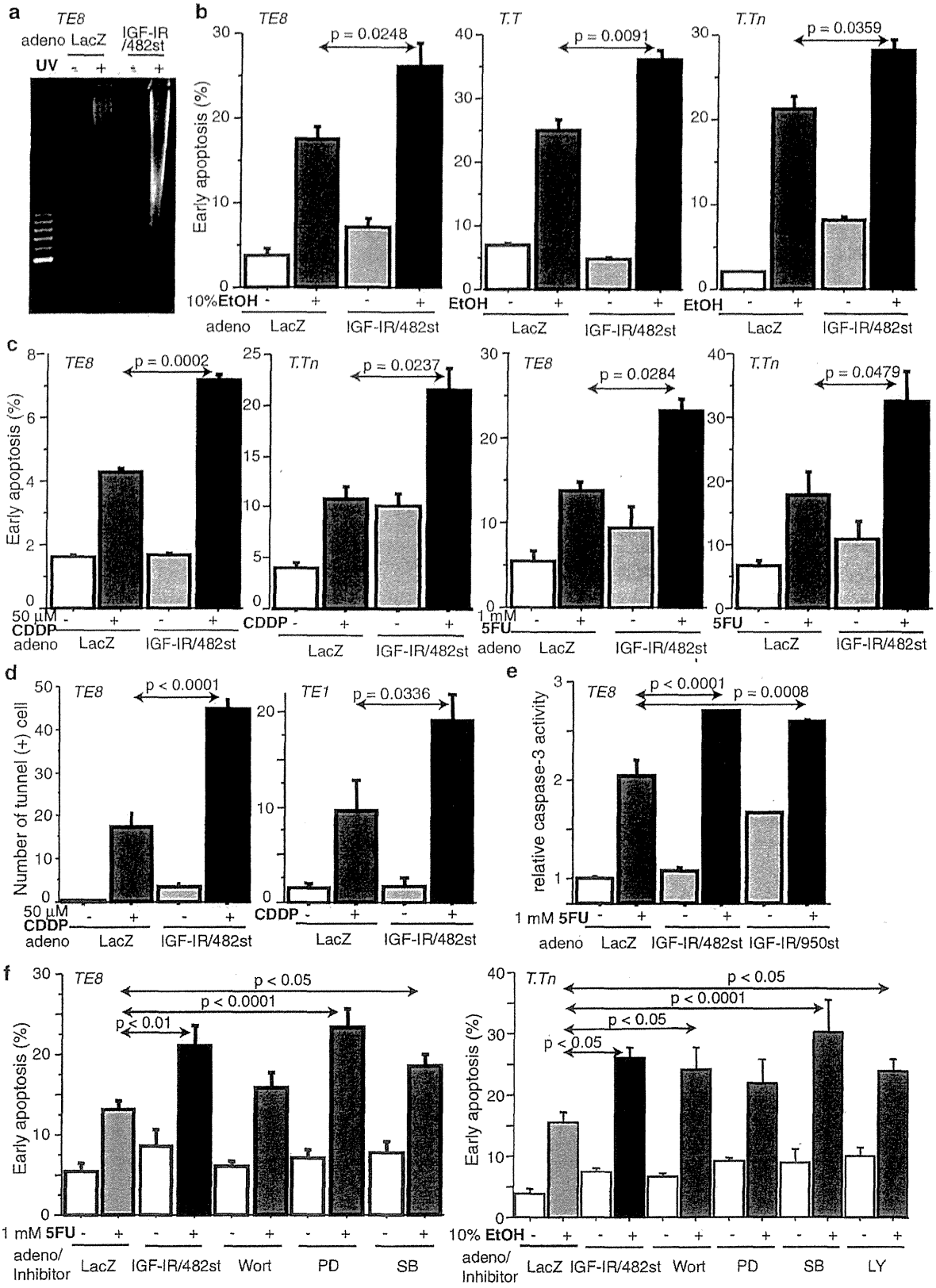
a
TE8
adeno LacZ
IGF-IR /482st
UV
b
TE8
T.T
T.Tn
p = 0.0248
p = 0.0091
p = 0.0359
Early apoptosis (%)
10%EtOH
EtOH
adeno LacZ IGF-IR/482st
c
TE8
T.Tn
p = 0.0002
p = 0.0237
p = 0.0284
p = 0.0479
Early apoptosis (%)
50 μM CDDP
1 mM 5FU
adeno LacZ IGF-IR/482st
d
TE8
TE1
p < 0.0001
p = 0.0336
Number of tunnel (+) cell
50 μM CDDP
adeno LacZ IGF-IR/482st
e
TE8
p < 0.0001
p = 0.0008
relative caspase-3 activity
1 mM 5FU
adeno LacZ IGF-IR/482st IGF-IR/950st
f
TE8
T.Tn
p < 0.05
p < 0.0001
p < 0.01
p < 0.05
Early apoptosis (%)
1 mM 5FU
10% EtOH
adeno/ Inhibitor
LacZ IGF-IR/482st Wort PD SB LY

◀ **Fig. 5** Apoptotic induction in ESCC. **a** DNA fragmentation assay showed UV-induced apoptosis. **b** Annexin-V assay revealed ethanol (EtOH)-induced early apoptosis. **c** Cells were treated with chemotherapy for 24 h. Then, annexin-V assay detected early apoptosis. **d** TUNEL assay revealed cisplatin-induced apoptosis. **e** Caspase-3 assays demonstrated 5-FU-induced apoptosis. **f** Annexin-V assay detected early apoptosis in ESCC cells with several inhibitors or IGF-IR/dn

Statistical analysis

Statistical significance of difference between IGF-IR expressions was determined by Fisher's exact probability test.

The results of in vitro experiments are presented as means ± SE for each sample. The statistical significance of difference was determined by one-way ANOVA or two-factor factorial ANOVA. *P* values less than 0.05 were considered to indicate statistical significance.

Results

The expressions of IGF axis in esophageal cancers

In the previous paper, we reported that many ESCC cell lines express both IGF-IR and IGF-II, but a few cells express IGF-I [21]. We evaluated the mRNA expression of both IGF-IR and its ligands in two esophageal adenocarcinoma cell lines using RT-PCR (Fig. 1a). Like the control ESCC, TE1, both IGF-IR and IGF-II messages were identified. However, none expressed IGF-I mRNA. Then, we assessed the protein expressions of both IGF-IR and InsR using Western blotting (Fig. 1b). Both receptors were expressed in the two adenocarcinoma cell lines, and those expression levels were less than those of four ESCC lines.

Tissue array data showed that IGF-IR was expressed in cancer tissue more frequently than the normal mucosa (54 and 0%, respectively, $p = 0.0111$; Table 1). The expression of IGF-IR tended to be lower in EAC compared to ESCC (eight out of 22 primary EAC and 15 of 23 primary EACC). In ESCC, the IGF-IR expression ratio of metastatic sites tended to be higher, but not significantly so than that of the primary sites (73 and 65%, respectively).

These results indicate that both ligands and receptors are expressed in many esophageal carcinomas, implying that the IGF/IGF-IR axis might play some role in not only ESCC but also EAC.

The effect of IGF-IR blockade on EAC cell lines

The natural inhibitor of IGFs, IGFBP3, suppressed the growth of OE33 to a similar level as that observed when they are cultured in serum-free media (Fig. 2a). Ad-IGF-IR/dn could reduce in vitro cell growth of both OE33 and OE19 (Fig. 2b). WST-1 assay showed that IGF-IR/dn blocked the growth of OE33 on plastic in a dose-dependent manner (Fig. 2c). IGF-IR/dn also reduced the number of colonies in a dose-dependent manner and strengthened the suppressive effect of cisplatin on colony formation of OE33 (Fig. 2d). Moreover, silencing IGF-IR by ad-shIGF-IR reduced colony number in a dose-dependent manner and enhanced cisplatin-induced suppression of colony formation in OE33 tumor cells.

Signaling analysis by Western blotting showed that ad-IGF-IR/dn could block both IGF-I- and IGF-II-induced phosphorylation of Akt in OE33 (Fig. 2e). IGF-IR/dn also reduced phosphorylation of both ERKs and S6. IGF-IR/dn could block des(1–3)IGF-I induced downstream signal transduction but not insulin-derived signals.

DNA fragmentation assays showed that IGF-IR/dn induced apoptosis in OE33 (Fig. 2f). In addition, IGF-IR/dn could enhance UV-induced apoptosis in OE33. The results were confirmed in another EAC cell, OE19. Moreover, ad-shIGF-IR showed almost the same effect as ad-IGF-IR/dn in both cell lines. Caspase-3 assays revealed that IGF-IR/dn up-regulated cisplatin-induced apoptosis in both OE33 and OE19 (Fig. 2g).

The results indicate that blockade of IGF-IR suppressed growth and colony formation and induced apoptosis in EAC cells.

The effect of IGF-IR/dn on ESCC cell growth

In the previous report, we showed the effects of IGF-IR/dn mainly for the ESCC cell line, TE1, so here we assessed the effect of IGF-IR blockade on several other ESCC cell lines as well [21].

IGF-BP3 suppressed proliferation of TE1 cultured in conditioned media with serum (Fig. 3a). The cell growth was markedly suppressed in the media without serum and IGF-I partially overcame this suppression. IGF-IR/482st suppressed in vitro growth of other ESCC cell lines, TE8, T.T, and T.Tn, in addition to TE1 (Fig. 3b). In every cell line, IGF-IR/dn was the most effective for growth suppression among tested inhibitors, wortmannin, LY294002, PD98059, and SB203580.

Soft agar assays revealed that IGF-IR/482st inhibited in vitro tumorigenicity in three ESCC cells: TE8, T.T, and T.Tn (Fig. 3c). In addition to IGF-IR/482st, another dominant negative, IGF-IR/950st, suppressed the carcinogenicity of T.Tn. Colony formation assays showed that IGF-IR/482st suppressed colony formation in a dose-dependent manner (Fig. 3d).

IGF-IR/dn blocked signal transduction in ESCC cell lines

Both IGF-I and IGF-II could induce phosphorylation of Akt-1 in both TE1 and TE8 cells (Fig. 4a). Effective concentrations of IGF-I were from 5 to 100 ng/ml, and IGF-II was also effective from 5 to 100 ng/ml. In both cell lines, 5 ng/ml IGF-I and 10 ng/ml IGF-II resulted in the activation of Akt-1 in 2.5 to 20 min (Fig. 4b).

Both Akt-1 and ERKs were phosphorylated by the ligands, IGF-I and IGF-II, in TE8 infected with control virus; however, Akt activation was blocked in the cells infected with IGF-IR/482st (Fig. 4c). The same results were observed in the other cell lines, TE1, T.T, and T.Tn (Fig. 4d–f). In the latter two cell lines, IGF-IR/482st inhibited the ligand-induced phosphorylation of S6. In T.Tn, des(1–3)IGF-I phosphorylated both downstream of Akt-1 and ERKs (Fig. 4g). In addition to IGF-IR/482st, IGF-IR/950st blocked phosphorylation of Akt-1 but not ERK in T.Tn.

Up-regulation of apoptotic induction on ESCC cell lines by IGF-IR/dn

DNA fragmentation assays revealed that the expression of IGF-IR/dn induced up-regulation of UV-induced apoptosis in TE8 (Fig. 5a). Annexin-V assays showed that IGF-IR/dn up-regulated 10% ethanol-induced early apoptosis in three cell lines, TE8, T.T, and T.Tn (Fig. 5b). Moreover, IGF-IR/dn increased apoptosis induced by both chemotherapies (cisplatin and 5-FU) in both TE8 and T.Tn (Fig. 5c). TUNEL assays confirmed the result that IGF-IR/482st enhanced cisplatin-induced apoptosis in both TE8 and TE1 (Fig. 5d). Both IGF-IR/482st and IGF-IR/950st up-regulated 5-FU-induced apoptosis in TE8 as detected by caspase-3 assays (Fig. 5e).

Both PD98059 and SB203580 up-regulated 5-FU-induced apoptosis in TE8 but wortmannin could not, as detected by annexin-V assays (Fig. 5f). Three inhibitors, wortmannin, LY294002, and SB203580, enhanced 10% ethanol-induced early apoptosis in T.Tn, but PD98059 did not.

The effect of IGF-IR on the migration of ESCC cell lines

T.T cells exhibited high mobility when cultured on plastic in a conditioned medium, but migration was reduced when these cells were cultured without serum (Fig. 6a). IGF-I stimulated the mobility of T.T in a dose-dependent manner, and IGFBP-3 reduced the migration ability of T.T cultured in conditioned media with FCS. The results indicated that the IGF/IGF-IR axis might play a part in the mobility of ESCC.

Both IGF-IR/dns suppressed the migration of T.T significantly (Fig. 6b). Moreover, both forms of IGF-IR/dn reduced the mobility of the other two cell lines, TE8 and T.Tn.

The effect of BMS-536924 for both types of esophageal carcinoma

The IGF-IR/InsR inhibitor, BMS-536924, blocked IGF-I-induced IGF-IR auto-phosphorylation and its down-stream signals, pAkt and pERKs, in an ESCC cell, TE8 (Fig. 7a). The same results were detected in an EAC cell, OE33. Compared to IGF-IR/dn, BMS-536924 could also block the phosphorylation of ERKs clearly in both cell lines.

BMS-536924 inhibited insulin-induced InsR autophosphorylation and activation of not only Akt but also ERKs in both cell types (Fig. 7b), unlike IGF-IR/482st and IGF-IR/950st.

The kinase inhibitor suppressed colony formation of TE8 completely and blocked that of OE33 in a dose-dependent manner (Fig. 7c). Caspase-3 assay showed that BMS-536924 enhanced 5FU-induced apoptosis in a dose-dependent manner (Fig. 7d).

The results indicate that IGF-IR target therapy might be a candidate strategy for both types of esophageal carcinomas.

Discussion

We show here that EAC cell lines express both IGF-II and IGF-IR, but not IGF-I, similar to ESCC. We also showed that IGF-IR was expressed in metastatic deposits in addition to the primary ESCC tumors. EAC expressed IGF-IR but tended to do so less frequently than ESCC. These results are compatible with the recent report in which higher IGF-IR protein expressions were observed in ESCC cells compared with EAC cells

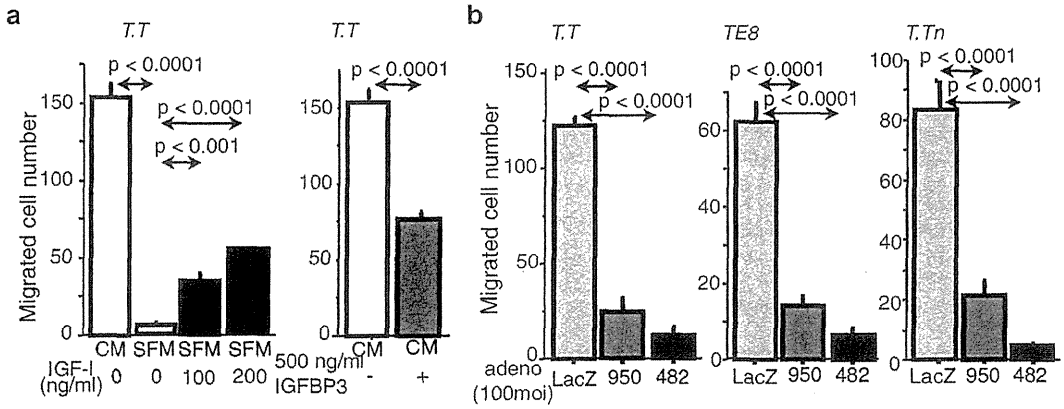

Fig. 6 The effect of IGF axis on migration of ESCC assessed by wounding assays. **a** TT cells were cultured with or without FBS ± IGF-I for 24 h and were cultured with/without IGFBP3. **b** Migration assay was performed for adenoviruses-infected cells

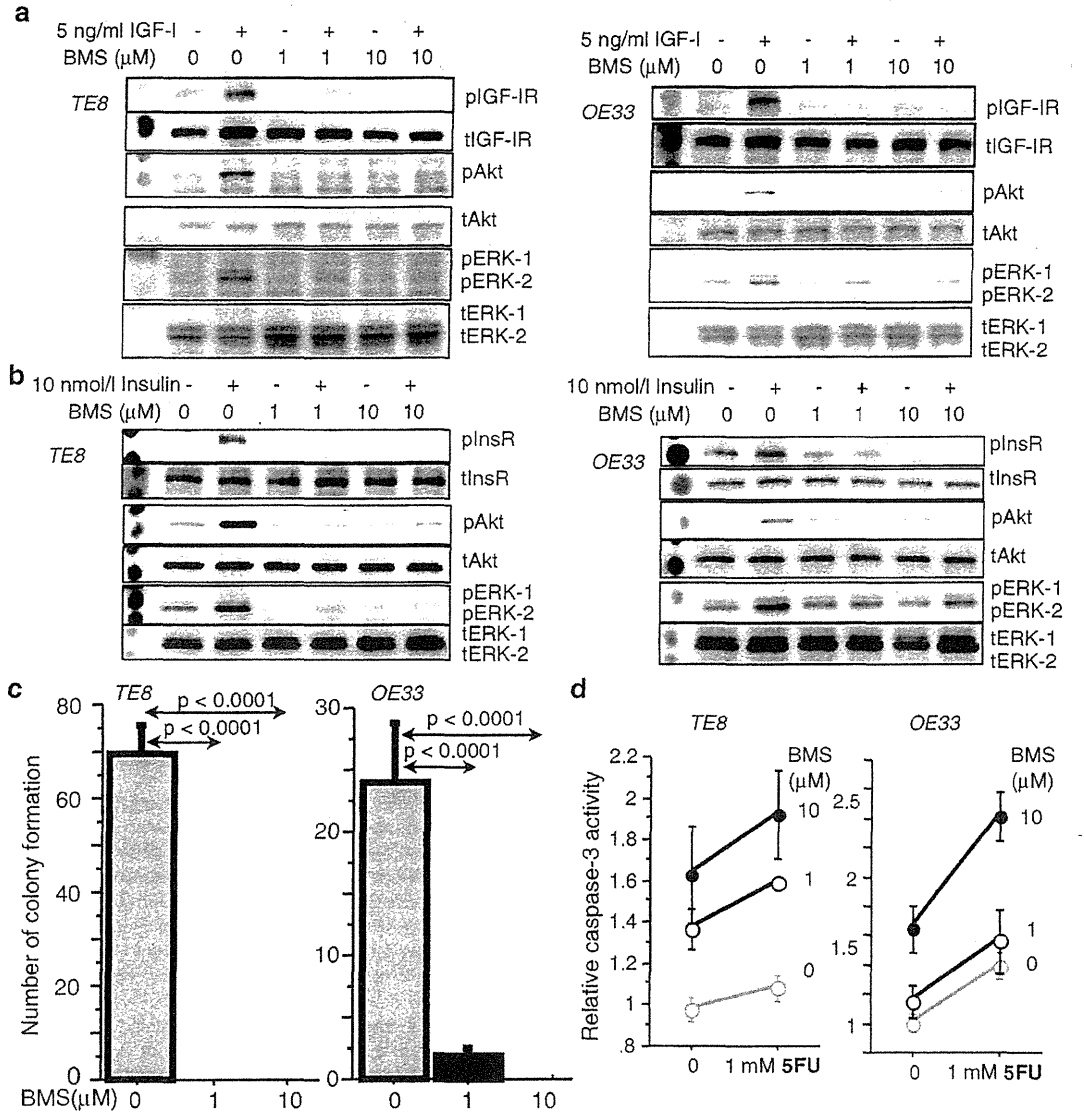

Fig. 7 The effect of BMS-536924 on both ESCC, TE8 and EAC, OE33. **a** After the cell was cultured with several amounts of BMS-536924, cells were stimulated for 5 min with IGF-I. Then Western blotting was performed. **b** After BMS-536924 treatment, the cells were stimulated for 5 min with insulin. **c** Colony formation assay revealed that this inhibitor reduced the number of colonies. **d** Caspase-3 assay revealed 5-FU-induced apoptosis

[22]. IGF-IR expression could also be useful as a novel prognostic marker for EAC [42]. Thus, IGF-IR might be a therapeutic target for many esophageal carcinomas.

In our previous study, we demonstrated that the IGF-IR axis is not only frequently overexpressed in ESCC and is associated with poor outcome but that it is also an exciting potential target for therapeutic intervention in this specific disease [21]. One of the possible mechanisms of IGF-IR overexpression in ESCC is that the miR-375 is downregulated by promoter methylation as miR-375 has a strong tumor-suppressive effect through inhibiting the expression of IGF-IR [43].

In this study, ad-IGF-IR/dn suppressed in vitro tumorigenicity, survival, and migration of both ESCC and EAC cells and also enhanced chemotherapy-induced apoptosis. In several cell lines representative of the two esophageal cancer subtypes (that express different patterns of IGF-IR and IGF ligand expression), the effects of ad-IGF-IR/dns were very similar, suggesting that IGF-IR targeting might have therapeutic potency for a variety of patients with esophageal carcinomas. This is also supported by the results from the multiple different inhibitors used in this study: IGF-IR/dns, shIGF-IR, and BMS-536924 all showed tumor-suppressive effects for esophageal carcinomas.